RESEARCH ARTICLE

National Science Open
5: 20260003, 2026
https://doi.org/10.1360/nso/20260003

Materials Science

Special Topic: Hollow Multishelled Structure

Cavity engineering of amorphous zeolitic imidazolate framework colloids and their core-shell architectures

Wei Zhang[1,2,*] & Nicola Pinna[2,*]

[1]*Key Laboratory of Organic Compound Pollution Control Engineering (Ministry of Education), School of Environmental and Chemical Engineering, Shanghai University, Shanghai 200444, China;*
[2]*Department of Chemistry and The Center for the Science of Materials Berlin, Humboldt-Universität zu Berlin, Berlin 12489, Germany*

*Corresponding authors (emails: weizhang88@shu.edu.cn (Wei Zhang); nicola.pinna@hu-berlin.de (Nicola Pinna))

Received 6 January 2026; Revised 21 January 2026; Accepted 30 January 2026; Published online 1 February 2026

Abstract: Metal-organic frameworks (MOFs), as a class of typical crystalline porous solids, have been extensively studied and applied in various fields, including gas adsorption and separation, catalysis, and chemical sensing. Recently, compared to their crystalline counterparts, the amorphous states of MOFs have attracted growing interest because they possess unique properties such as mechanical robustness, stability, molecular selectivity, and processability. However, the direct synthesis of amorphous MOF colloids remains a significant challenge, particularly for fabricating complex micro- and nanostructures such as hollow or yolk-shell architectures. Herein, we develop a simple strategy to synthesize hollow structures in amorphous zeolitic imidazolate framework (ZIF) colloids through controlled post-synthetic etching. Tannic acid, functioning as a proton etching agent, was utilized to achieve selective dissolution of the inner region in pre-formed monodisperse amorphous ZIF colloids, forming a uniform hollow structure. This etching process has been successfully demonstrated across various ZIFs, providing strong evidence of the method's universality for ZIF systems. Furthermore, this method can also be applied to the synthesis of conformal yolk-shell structures by precisely etching the core-shell structure. The synthesized hollow ZIF nanoparticles hold great potential for applications across diverse fields, including catalysis and drug delivery. More importantly, this method pioneers a new pathway for cavity engineering of amorphous MOF colloids.

Keywords: metal organic frameworks, hollow nanostructures, amorphous, zeolitic imidazolate framework

INTRODUCTION

Metal-organic frameworks (MOFs) are porous crystalline materials featuring periodic network structures formed by metal nodes connected via coordinate bonds with organic ligands [1–3]. Their exceptionally high specific surface area, highly tunable pore structures, molecular-level design flexibility, and accessible metal active sites confer significant application potential in gas storage and separation [4], catalysis [5–8], energy storage [9–13], sensing [14,15], and biomedical fields [16,17]. Currently, crystalline MOFs remain the research mainstream in this field, but amorphous MOFs, especially MOF glass, have gradually gained attention in recent years [18,19]. Through the typical melting-quenching or ball-milling process, crystalline MOFs can form a glass [18]. MOF glasses, with their organic-inorganic hybrid nature, differ from con-

ventional inorganic, organic, and metallic glasses, representing a distinct fourth category of glass materials. Compared to crystalline forms, glassy MOFs could exhibit unique properties such as higher mechanical strength, excellent stability, superior molecular selectivity, and processability [20–25].

Amorphous MOF colloids or nanoparticles, which offer greater flexibility in the choice of metals and ligands, represent another vital component of the non-crystalline MOF material system. Typically synthesized via mild bottom-up strategies, these materials enable precise control over their micro- and nanostructures, demonstrating unique advantages in fields such as optics [26], drug delivery [27], and catalysis [28,29]. For instance, heterojunctions made from amorphous MOFs exhibit not only more uniform interfaces but also expose a greater number of unsaturated metal sites, thereby achieving higher catalytic activity [28,29]. In addition, amorphous ZIFs exhibit outstanding sustained-release properties in drug delivery, primarily due to controlled release pathways formed by the collapse of their ordered channels [27]. Furthermore, the inherently homogeneous and isotropic structure of amorphous MOF microspheres provides a unique foundation for optical applications [26]. However, the collapse of the internal ordered structure within amorphous MOFs reduces their intrinsic porosity, hindering mass transfer rates between the material's interior and exterior and consequently limiting overall performance enhancement. To address this issue, introducing a cavity into amorphous MOFs (e.g., by synthesizing hollow or yolk-shell structures) represents an effective strategy. Nevertheless, the hollow synthesis of amorphous MOF colloids or composite structures still faces significant challenges.

Here, we propose a post-synthetic etching method to create a cavity within amorphous MOF colloids (Figure 1). Compared to the one-step synthesis method, the post-etching strategy enables more precise control over the final morphology and pore structure of colloidal materials. This approach separates "material synthesis" and "structural refinement" into distinct steps: first synthesizing a basic precursor, then selectively etching it to "trim" its microstructure. This sequential processing grants the method greater flexibility in morphology control and pore design. Briefly, monodisperse amorphous zeolite imidazole framework-7 (aZIF-7) microspheres with a particle size of 200–300 nm were synthesized via the vapor diffusion method [30]. Subsequently, tannic acid was added to aZIF-7 suspension, resulting in a higher internal etching rate than the external surface, thereby forming a uniform hollow structure. During this process, tannic acid served a dual role as both an etchant and a protective agent: it preferentially adsorbed onto the microsphere surface, effectively inhibiting surface etching and enabling selective internal dissolution. This strategy proved equally effective for other amorphous ZIF systems (e.g., Zn-imidazole and Zn-5-chlorobenzimidazole systems), demonstrating excellent universality. Extending this method to suspensions of core-shell structures coated with amorphous MOFs could yield uniform yolk-shell structures. Moreover, other functional architectures, such as carbon-based yolk-shell composites, can also be synthesized through direct solid-state transformation. This post-etching strategy provides a novel synthetic approach for precise pore and structural control of amorphous MOF colloids.

RESULTS AND DISCUSSION

ZIF-7 is a metal-organic framework material formed by the coordination of zinc ions with benzimidazole units, wherein each zinc ion is connected to four deprotonated benzimidazole molecules (Figure 2a). This

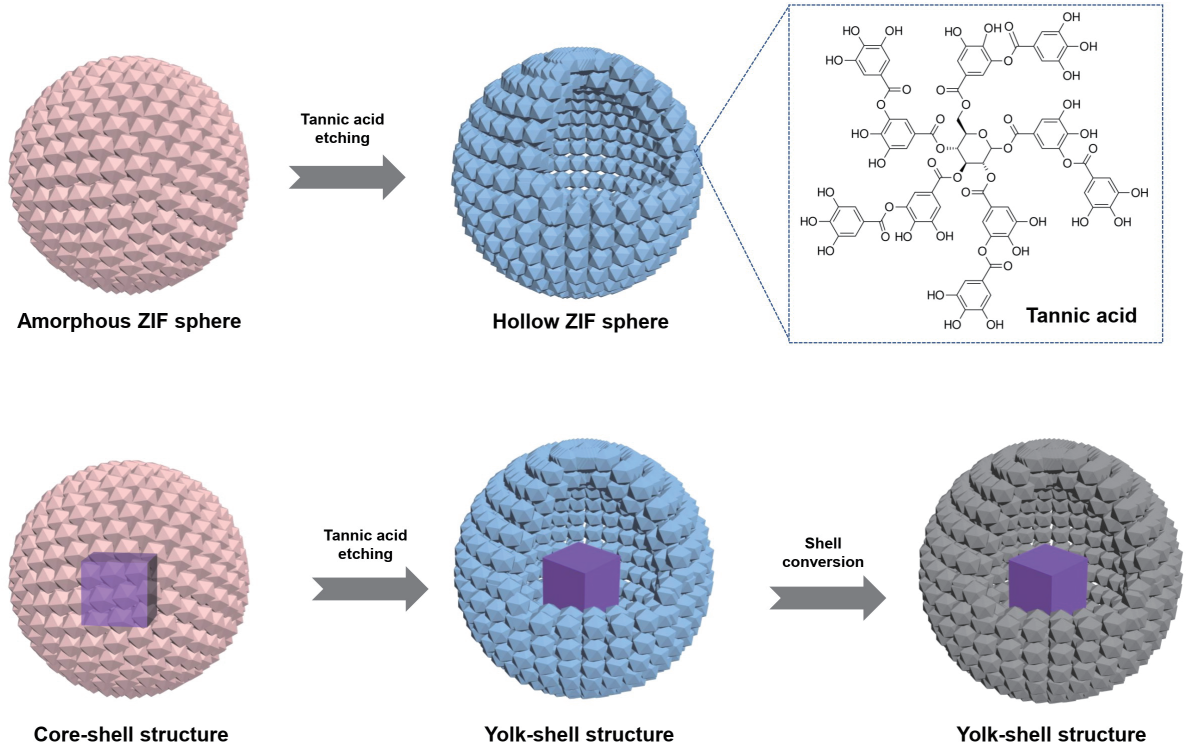

Figure 1 Schematic illustration of engineering of amorphous zeolitic imidazolate framework colloids and their core-shell architectures.

study synthesized amorphous ZIF-7 nanospheres via the triethylamine vapor diffusion method [30]. Scanning electron microscopy (SEM) image reveals that the prepared ZIF-7 nanospheres exhibit a size range of 200–300 nm with a distinct spherical morphology (Figure 2b and Figure S1). Transmission electron microscopy (TEM) images further confirm that these nanospheres possess a solid structure without noticeable internal voids (Figure 2c). The average shell thickness of hollow ZIF-7 is around 33 nm. As shown in Figure 2d, e and Figures S2 and S3, after tannic acid etching, the overall morphology of the ZIF-7 nanospheres remained unchanged, retaining their spherical shape, though surface roughness increased. Moreover, TEM images revealed that the central regions of the ZIF-7 nanospheres had been removed, forming hollow structures. This indicates that tannic acid selectively etches the internal regions of the ZIF-7 nanospheres. This phenomenon can be attributed to tannic acid's dual role as both a protective agent and an etchant during this process. Its strong adhesive properties enable rapid adsorption onto the ZIF-7 nanosphere surface to form a protective layer. Simultaneously, protons diffuse inward, resulting in a higher etching rate internally than externally, ultimately forming a hollow structure. This mechanism is consistent with the tannic acid etching of other crystalline MOF materials [31,32].

In the powder X-ray diffraction (PXRD) pattern, the initial ZIF-7 nanospheres exhibit a broad diffuse peak near 19°, indicating their amorphous structural characteristics (Figure 2g). After tannic acid etching, the resulting hollow spheres retain their original amorphous structure. Figure 2f shows the Fourier transform infrared (FT-IR) spectra. Comparison reveals that the hollow ZIF-7 retains the characteristic absorption peaks of the original ZIF-7 while exhibiting several new peaks originating from tannic acid at 1706, 1344, and 1031 cm^{-1} [33]. These new peaks correspond to the C=O stretching vibration, the asymmetric C–O

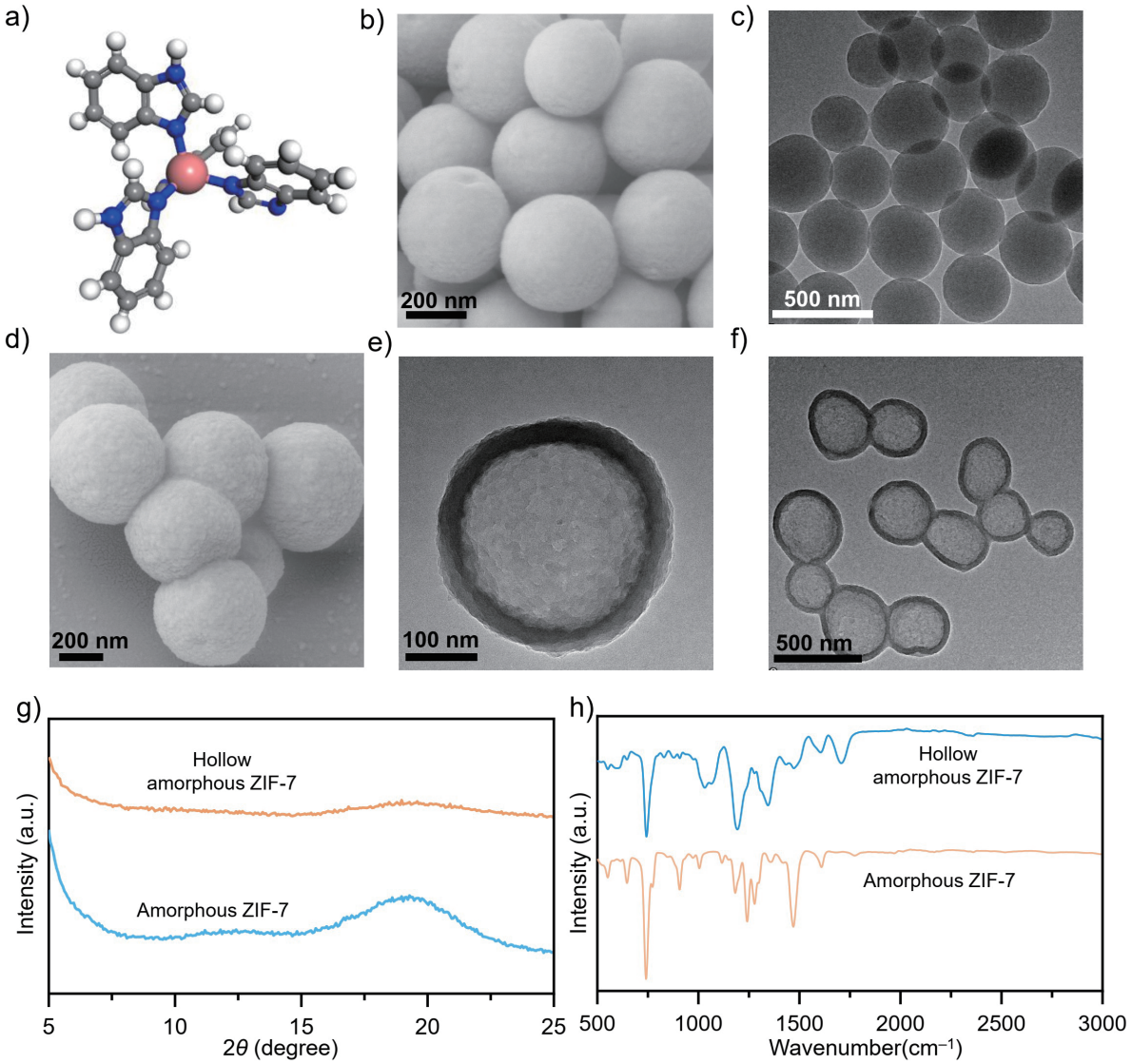

Figure 2 Characterizations of hollow ZIF-7 sphere. (a) Molecular structure of Zn-benzimidazole complex. Red spheres, zinc; grey, carbon; blue, nitrogen; white, hydrogen. (b) SEM image of solid amorphous ZIF-7. (c) TEM image of solid amorphous ZIF-7. (d) SEM image of hollow amorphous ZIF-7. (e, f) TEM images of hollow amorphous ZIF-7. (g) PXRD patterns of pristine and hollow amorphous ZIF-7. (h) FT-IR spectra of pristine and hollow amorphous ZIF-7.

stretching vibration of the aromatic ring, and the C–O–C stretching vibration in tannic acid, respectively [34], indicating that tannic acid has successfully adsorbed onto the surface of the hollow nanospheres.

To validate the universality of this etching method for preparing amorphous hollow ZIF nanospheres, we further selected other ZIFs for etching experiments. Figure 3a and Figure S4 indicate that solid Zn-imidazole nanospheres were successfully converted into hollow structures after tannic acid etching. The average shell thickness of hollow Zn-imidazole is 16 nm. Similarly, selective removal of the internal regions was also observed in Zn-5-chlorobenzimidazole nanospheres after etching, resulting in hollow structures (Figure 3b, Figures S5 and S6). These results demonstrate that this post-etching strategy holds promise for extension to additional amorphous ZIF systems. Further TEM elemental distribution analysis revealed that the resulting

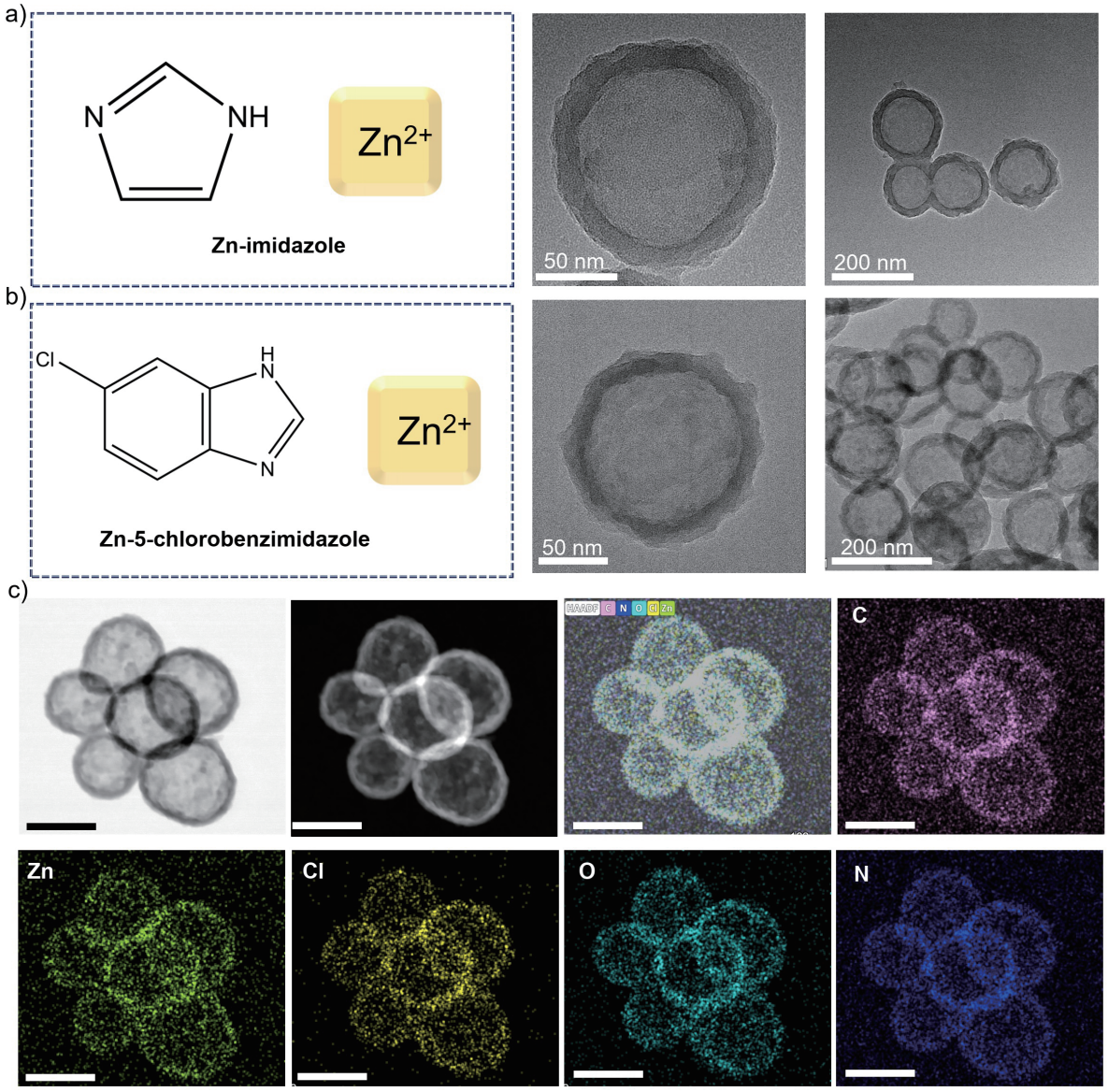

Figure 3 Extension to various zeolite imidazole frameworks. (a) TEM images of hollow Zn-imidazole spheres. (b) TEM images of hollow Zn-5-chlorobenzimidazole spheres. (c) Bright field STEM image, high-angle annular dark field scanning transmission electron microscopy (HAADF-STEM) image and element mapping images of hollow Zn-5-chlorobenzimidazole spheres. The scale bars are 100 nm.

hollow spheres comprise Zn, C, N, O, and Cl elements. Among these, Zn, N, and Cl primarily originate from the ZIF precursor, while O derives from tannic acid (Figure 3c and Figure S6c). Uniform distribution of all elements within the hollow shell demonstrates excellent structural homogeneity of this hollow sphere.

Beyond hollow structures, we further explored this method for synthesizing more complex architectures based on tannic acid etching. First, we uniformly coated Prussian blue cubes with a Zn-5-chlorobenzimidazole shell layer [30]. As shown in Figure 4a and Figure S7, the amorphous Zn-5-chlorobenzimidazole uniformly covered the Prussian blue surface, forming a conformal core-shell structure. Using this core-shell nanoparticle as a precursor, controlled tannic acid etching successfully transformed it into a yolk-shell structure (Figure 4b and Figure S8). The formation mechanism is similar to the previously

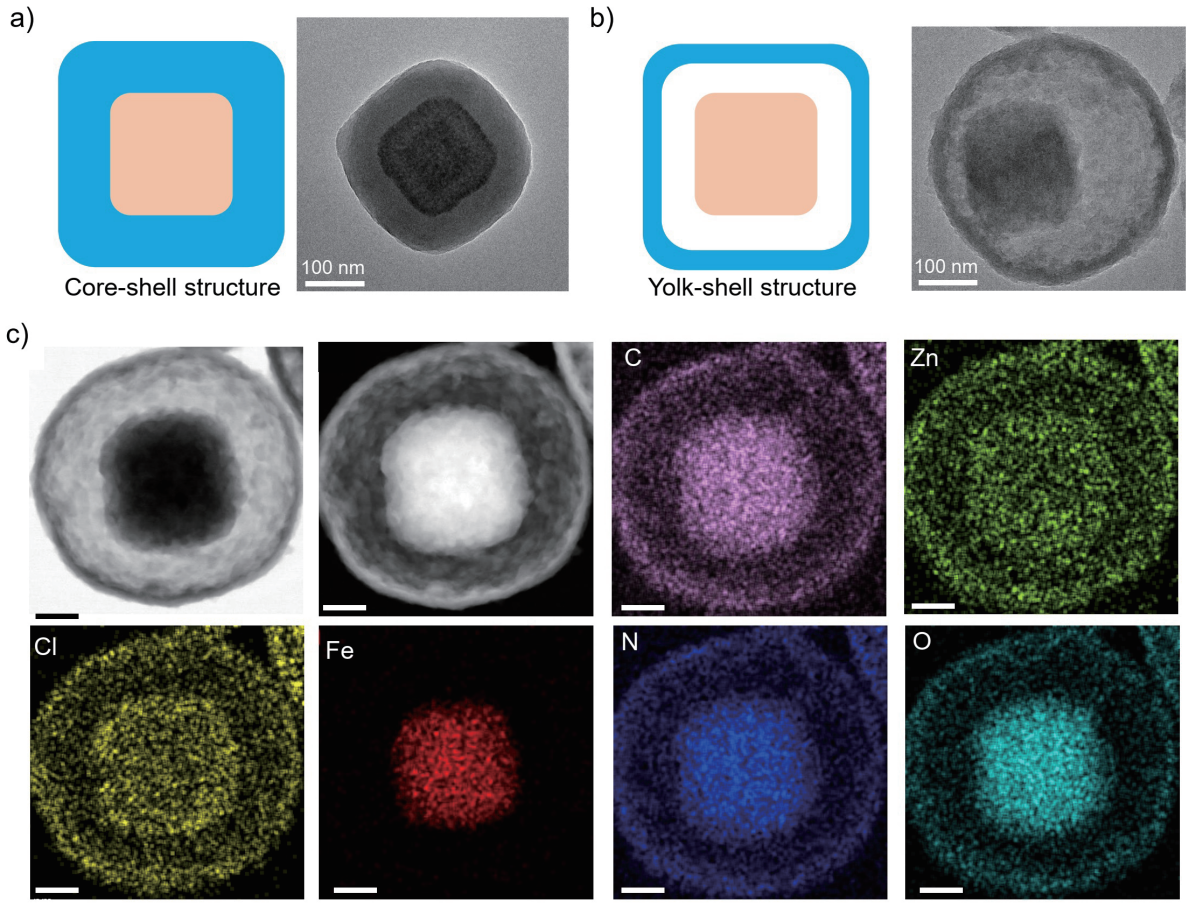

Figure 4 Characterizations of yolk-shell Zn-5-chlorobenzimidazole architecture. (a) TEM image of PB@ Zn-5-chlorobenzimidazole core-shell structure. (b) TEM image of PB@Void@Zn-5-chlorobenzimidazole yolk-shell structure. (c) Bright field STEM image, HAADF-STEM image and element mapping images of hollow PB@Void@Zn-5-chlorobenzimidazole yolk-shell structure. The scale bars are 50 nm.

described hollow structure. The internal ZIF region was rapidly etched away, while the outer shell layer was preserved under tannic acid protection, ultimately forming the yolk-shell structure. The elemental distribution mapping images in Figure 4c further confirm the structure's characteristics. Fe elements are exclusively distributed within the central cubic region, indicating their origin from the pristine Prussian blue core. Conversely, Zn and Cl elements predominantly reside in the outer shell, confirming the shell layer as an amorphous ZIF material. These results demonstrate that this method can successfully produce complex yolk-shell structures based on amorphous ZIFs.

Using the aforementioned method, we successfully synthesized β-FeOOH@Void@Zn-imidazole and Si@Void@ Zn-imidazole yolk-shell nanoparticles with a conformal structure (Figure 5a, b, Figures S9 and S10). The synthesis of micron-sized silicon-based yolk-shell structures has been a critical focus in lithium-ion batteries [35]. The internal void space in such structures can effectively accommodate the volume expansion of silicon during lithiation, thereby enhancing electrode stability. However, the synthesis of these architectures remains challenging. As shown in Figure 5b and Figure S10, irregular micron-sized silicon particles were uniformly encapsulated within the yolk-shell structure. Subsequently, under an argon protective atmosphere, the ZIF shell was converted into porous carbon via high-temperature pyrolysis. After

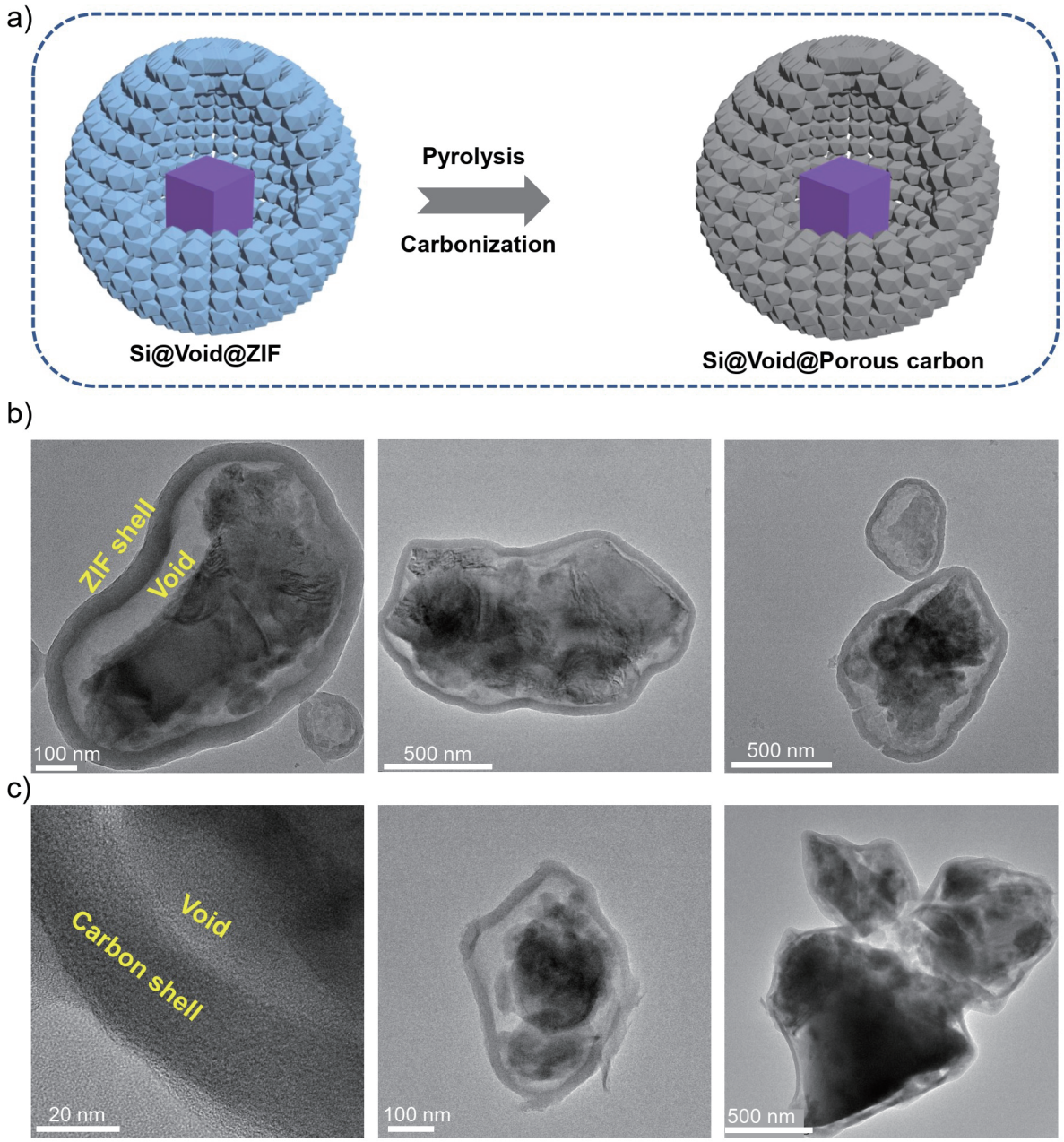

Figure 5 Solid-phase transformation of zeolite imidazole framework architecture. (a) Schematic illustration of conversion of yolk-shell structure from amorphous ZIF shell to porous carbon shell. (b) TEM images of Si@Void@Zn-imidazole yolk-shell nanoparticles. (c) TEM images of Si@Void@Porous carbon yolk-shell nanoparticles.

pyrolysis, the fundamental yolk-shell architecture was preserved, with only the shell layer transforming from ZIF into porous carbon. The porous carbon shell not only alleviates the volume expansion issue of silicon electrodes but also enhances the conductivity of the system and accelerates electron transfer rates, thereby facilitating the development of high-performance lithium-ion battery anodes. This solid-state conversion process successfully produced Si@Void@Carbon nanostructures (Figure 5c and Figure S10), further expanding the application potential of this method for preparing complex yolk-shell materials. Compared to

crystalline ZIFs, amorphous ZIFs are not constrained by crystalline periodicity, enabling more flexible integration with nanomaterials to form conformal core-shell architectures. This characteristic is particularly advantageous for coating irregularly shaped micrometer-sized particles. In yolk-shell structures, the uniformity of the shell plays a critical role in enhancing their performance for catalytic and energy storage-related applications.

CONCLUSIONS

This study successfully developed a universal strategy based on selective tannic acid etching, enabling the efficient synthesis of various hollow and yolk-shell structures based on amorphous ZIF materials. Experiments demonstrate the universality of this approach across diverse amorphous ZIF systems, including ZIF-7, Zn-imidazole, and Zn-5-chlorobenzimidazole. It enables directional etching of internal regions while preserving external morphology, yielding structurally intact hollow nanospheres. Furthermore, this method can be extended to synthesize complex heterogeneous structures. Using Prussian blue@ZIF core-shell structures as precursors, controlled etching successfully produced yolk-shell architectures whose structural integrity was verified through elemental distribution analysis. Moreover, high-temperature pyrolytic conversion transformed the ZIF shell into porous carbon, enabling the synthesis of other functional yolk-shell materials like Si@Void@Carbon. This demonstrates the method's flexibility and application potential in material design and functionalization. In summary, this study not only provides a simple, controllable synthesis pathway for hollowing and producing complex structures in amorphous ZIFs, but also lays the foundation for subsequent functional material development based on hollow/yolk-shell architectures.

Data availability

All data generated during this work are included in this published article.

Funding

W.Z. acknowledges the Alexander von Humboldt Foundation, Bonn, Germany for a postdoctoral fellowship and research grant. Open access funding enabled and organized by Projekt DEAL.

Author contributions

W.Z. conducted the investigation, carried out experiments, analyzed the data, and drafted the manuscript. W.Z. and N.P. offered insights regarding growth design and data analysis. W.Z. and N.P. refined the experimental design, and reviewed and revised the paper.

Conflict of interest

The authors declare no conflict of interest.

Supplementary information

The supporting information is available online at https://doi.org/10.1360/nso/20260003. The supporting materials are published as submitted, without typesetting or editing. The responsibility for scientific accuracy and content remains entirely with the authors.

References

1 Yaghi OM, O'Keeffe M, Ockwig NW, *et al.* Reticular synthesis and the design of new materials. *Nature* 2003; **423**: 705–714.

2 Kitagawa S, Kitaura R, Noro S. Functional porous coordination polymers. *Angew Chem Int Ed* 2004; **43**: 2334–2375.

3 Zhang W, Bojdys MJ, Pinna N. A universal synthesis strategy for tunable metal-organic framework nanohybrids. *Angew Chem Int Ed* 2023; **62**: e202301021.

4 Li JR, Kuppler RJ, Zhou HC. Selective gas adsorption and separation in metal-organic frameworks. *Chem Soc Rev* 2009; **38**: 1477–1504.

5 Feng D, Gu ZY, Li JR, *et al.* Zirconium-metalloporphyrin PCN-222: Mesoporous metal-organic frameworks with ultrahigh stability as biomimetic catalysts. *Angew Chem Int Ed* 2012; **51**: 10307–10310.

6 Jiao L, Jiang HL. Metal-organic-framework-based single-atom catalysts for energy applications. *Chem* 2019; **5**: 786–804.

7 Lee JY, Farha OK, Roberts J, *et al.* Metal-organic framework materials as catalysts. *Chem Soc Rev* 2009; **38**: 1450–1459.

8 Wei YS, Zhang M, Zou R, *et al.* Metal-organic framework-based catalysts with single metal sites. *Chem Rev* 2020; **120**: 12089–12174.

9 Wang C, Kaneti YV, Bando Y, *et al.* Metal-organic framework-derived one-dimensional porous or hollow carbon-based nanofibers for energy storage and conversion. *Mater Horiz* 2018; **5**: 394–407.

10 Wang L, Han Y, Feng X, *et al.* Metal-organic frameworks for energy storage: Batteries and supercapacitors. *Coord Chem Rev* 2016; **307**: 361–381.

11 Zhang W, Xia L, Shi C, *et al.* Casting and recycling of insoluble, labile single-crystal coordination polymer through reversible solid-liquid-solid transition. *Matter* 2023; **6**: 3394–3412.

12 Wan Z, Zhang W, Li T, *et al.* Automated nanoarchitectonics for networks filling by Prussian blue single crystals through an intermittentto-flow conversion. *Chem Eng J* 2025; **505**: 159525.

13 Zhang W, Chen W, Zhao X, *et al.* An auto-switchable dual-mode seawater energy extraction system enabled by metal-organic frameworks. *Angew Chem Int Ed* 2019; **58**: 7431–7434.

14 Mohanty B, Kumari S, Yadav P, *et al.* Metal-organic frameworks (MOFs) and MOF composites based biosensors. *Coord Chem Rev* 2024; **519**: 216102.

15 Sharma A, Eadi SB, Noothalapati H, *et al.* Porous materials as effective chemiresistive gas sensors. *Chem Soc Rev* 2024; **53**: 2530–2577.

16 Bigham A, Islami N, Khosravi A, *et al.* MOFs and MOF-based composites as next-generation materials for wound healing and dressings. *Small* 2024; **20**: 2311903.

17 Abánades Lázaro I, Chen X, Ding M, *et al.* Metal-organic frameworks for biological applications. *Nat Rev Methods Primers* 2024; **4**: 42.

18 Bennett TD, Horike S. Liquid, glass and amorphous solid states of coordination polymers and metal-organic frameworks. *Nat Rev Mater* 2018; **3**: 431–440.

19 Tao H, Bennett TD, Yue Y. Melt-quenched hybrid glasses from metal-organic frameworks. *Adv Mater* 2017; **29**: 1601705.

20 Bennett TD, Keen DA, Tan JC, *et al.* Thermal amorphization of zeolitic imidazolate frameworks. *Angew Chem Int Ed* 2011; **50**: 3067–3071.

21 Bennett TD, Tan JC, Yue Y, *et al.* Hybrid glasses from strong and fragile metal-organic framework liquids. *Nat Commun* 2015; **6**: 8079.

22 Li S, Limbach R, Longley L, *et al.* Mechanical properties and processing techniques of bulk metal-organic framework glasses. *J Am Chem Soc* 2019; **141**: 1027–1034.

23 Pallach R, Keupp J, Terlinden K, *et al.* Frustrated flexibility in metal-organic frameworks. *Nat Commun* 2021; **12**: 4097.

24 Frentzel-Beyme L, Kolodzeiski P, Weiß JB, *et al.* Quantification of gas-accessible microporosity in metal-organic

framework glasses. *Nat Commun* 2022; **13**: 7750.

25 Yang Z, Belmabkhout Y, McHugh LN, *et al.* ZIF-62 glass foam self-supported membranes to address CH_4/N_2 separations. *Nat Mater* 2023; **22**: 888–894.

26 Gao Z, Xu B, Fan Y, *et al.* Topological-distortion-driven amorphous spherical metal-organic frameworks for high-quality single-mode microlasers. *Angew Chem Int Ed* 2021; **60**: 6362–6366.

27 Wu X, Yue H, Zhang Y, *et al.* Packaging and delivering enzymes by amorphous metal-organic frameworks. *Nat Commun* 2019; **10**: 5165.

28 Mitsuka Y, Ogiwara N, Mukoyoshi M, *et al.* Fabrication of integrated copper-based nanoparticles/amorphous metal-organic framework by a facile spray-drying method: Highly enhanced CO_2 hydrogenation activity for methanol synthesis. *Angew Chem Int Ed* 2021; **60**: 22283–22288.

29 Liu C, Wang J, Wan J, *et al.* Amorphous metal-organic framework-dominated nanocomposites with both compositional and structural heterogeneity for oxygen evolution. *Angew Chem Int Ed* 2020; **59**: 3630–3637.

30 Zhang W, Liu Y, Jeppesen HS, *et al.* Stöber method to amorphous metal-organic frameworks and coordination polymers. *Nat Commun* 2024; **15**: 5463.

31 Hu M, Ju Y, Liang K, *et al.* Void engineering in metal-organic frameworks via synergistic etching and surface functionalization. *Adv Funct Mater* 2016; **26**: 5827–5834.

32 Zhang W, Jiang X, Zhao Y, *et al.* Hollow carbon nanobubbles: Monocrystalline MOF nanobubbles and their pyrolysis. *Chem Sci* 2017; **8**: 3538–3546.

33 Xia Z, Singh A, Kiratitanavit W, *et al.* Unraveling the mechanism of thermal and thermo-oxidative degradation of tannic acid. *ThermoChim Acta* 2015; **605**: 77–85.

34 Sarango L, Benito J, Gascón I, *et al.* Homogeneous thin coatings of zeolitic imidazolate frameworks prepared on quartz crystal sensors for CO_2 adsorption. *Microporous Mesoporous Mater* 2018; **272**: 44–52.

35 Li Y, Yan K, Lee HW, *et al.* Growth of conformal graphene cages on micrometre-sized silicon particles as stable battery anodes. *Nat Energy* 2016; **1**: 15029.